

## Enhanced Reference Stress Method for LBB Analysis

300

103-16

$J$ -integral and COD estimation equations, the results from published pipe test data are compared with the proposed ones. Furthermore, the  $J$ -integral and CODs predicted using the proposed method are also compared with those of based on three dimensional elastic-plastic finite element analyses. The results show good agreement with pipe test data and the 3-D FE data. The present results provide confidence in applying the proposed ERS method to the Leak-before-Break analysis.

### Abstract

This paper proposes the enhanced reference stress (ERS) method to estimate the elastic-plastic  $J$ -integral and crack tip opening displacement (COD) for circumferential through-wall cracked pipes. To validate the proposed COD estimation equations, the results from published pipe test data are compared with the proposed ones. Furthermore, the  $J$ -integral and CODs predicted using the proposed method are also compared with those of based on three dimensional elastic-plastic finite element analyses. The results show good agreement with pipe test data and the 3-D FE data. The present results provide confidence in applying the proposed ERS method to the Leak-before-Break analysis.

# 1.

(Leak-before-Break; LBB) . LBB  
 가  
 (Elastic-Plastic Fracture Mechanics; EPFM)  
 가  
 LBB Displacement; COD) EPFM J- (Crack Opening COD  
 , (engineering estimation scheme),  
 가  
 가  
 (reference stress method)[2] GE/EPRI [1]  
 Ramberg-Osgood 가 GE/EPRI (curve fitting)  
 가 [3]. GE/EPRI  
 가 R6 가 [4]  
 (plastic limit load) 가  
 J- COD  
 (Enhanced Reference Stress; ERS)  
 가 3  
 가 GE/EPRI[1,5]

## 2. ERS J- COD 가

### 2.1 J- COD 가

J- COD 가 2  
 가 2  
 , 1

#### 2.1.1 2 가

2 J- 가

$$\frac{J}{J_e} = \frac{Ee_{ref}}{s_{ref}} + \frac{1}{2} \frac{L_r^2 s_{ref}}{Ee_{ref}} \quad (1)$$

,  $J_e$  J-  $s_{ref}$   $e_{ref}$   
 ,  $L_r$

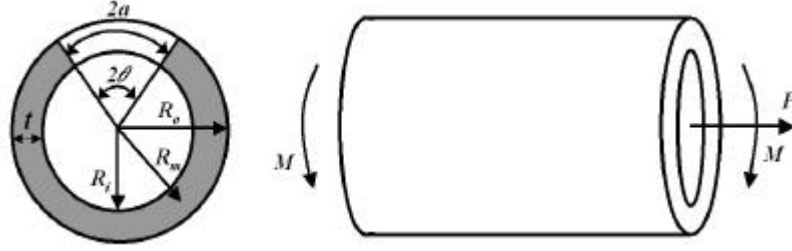


Fig. 1 Circumferential through-wall cracked pipes under axial tension and under bending

$$L_r = \mathbf{s}_{ref} / \mathbf{s}_y = P / P_o^* = M / M_o^* \quad (2)$$

,  $P$   $M$  ,  $P_o^*$   $M_o^*$  Fig. 1  
 $(P_L)$   $(M_L)$   
(optimised reference load) .

$$P_o^* = \mathbf{g}(\mathbf{q})P_L ; M_o^* = \mathbf{g}(\mathbf{q})M_L \quad (3)$$

$$\mathbf{g}(\mathbf{q}) = 0.82 + 0.75\left(\frac{\mathbf{q}}{\mathbf{p}}\right) + 0.42\left(\frac{\mathbf{q}}{\mathbf{p}}\right)^2 \text{ for } \mathbf{q}/\mathbf{p} \leq 0.5 \quad (4)$$

$$P_L = 2R_m t \mathbf{s}_y \left[ \mathbf{p} - \mathbf{q} - 2 \sin^{-1}\left(\frac{1}{2} \sin \mathbf{q}\right) \right] \quad (5)$$

$$M_L = 4R_m^2 t \mathbf{s}_y \left[ \cos\left(\frac{\mathbf{q}}{2}\right) - \frac{1}{2} \sin \mathbf{q} \right] \quad (6)$$

2 COD 가 .

$$\frac{\mathbf{d}}{\mathbf{d}_e} = \begin{cases} \frac{E \mathbf{e}_{ref}}{\mathbf{s}_{ref}} + \frac{1}{2} \frac{L_r^2 \mathbf{s}_{ref}}{E \mathbf{e}_{ref}} & \text{for } 0 \leq L_r \leq 1 \\ \left(\frac{\mathbf{d}}{\mathbf{d}_e}\right)_{L_r=1} (L_r)^{n_1-1} & \text{for } 1 < L_r \end{cases} \quad (7)$$

,  $\mathbf{d}_e$  COD  $(\mathbf{d}/\mathbf{d}_e)_{L_r=1}$   $L_r = 1$   $(\mathbf{d}/\mathbf{d}_e)$  .  
(7) 가  $n_1$  .

$$n_1 = \frac{\ln[(\mathbf{e}_{u,t} - \mathbf{s}_{u,t}/E)/0.002]}{\ln[\mathbf{s}_{u,t}/\mathbf{s}_y]} \quad (8)$$

,  $\mathbf{s}_{u,t}$   $\mathbf{e}_{u,t}$  (true tensile strength) .

2.1.2 1 가

(lower bound) 가

$$\frac{J}{J_e} = \left[ \frac{1}{(1 - 0.14L_r^2)(0.3 + 0.7 \exp(-0.65L_r^6))} \right]^2 \quad (9)$$

1 COD 가

$$\frac{d}{d_e} = \begin{cases} 1 + \frac{1}{2}L_r^2 & \text{for } L_r < 1 \\ \frac{3}{2}(L_r)^{n_2-1} & \text{for } L_r \geq 1 \end{cases} \quad (10)$$

,  $n_2$  ( $s_y/s_u$ )

$$1/n_2 = 0.629 - 1.536(s_y/s_u) + 1.723(s_y/s_u)^2 - 0.814(s_y/s_u)^3 \quad (11)$$

(10) (7) LBB 1 2 가 2 , COD

2.2 ERS J- COD 가

J- COD 가 [2] ERS J- COD 가

2.2.1 가

가 [2,4].

$$\mathbf{s}_{ref} = \begin{pmatrix} P \\ P_L \end{pmatrix} \mathbf{s}_y = \begin{pmatrix} M \\ M_L \end{pmatrix} \mathbf{s}_y \quad (12)$$

,  $P_L$   $M_L$  (5) (6) 가

[6].

J- COD 가

(3)

GE/EPRI

가

(3)

$P_o^*$

$M_o^*$  GE/EPRI (3) J- COD (3)  $P_o^*$  ( $h_1, h_2$ ) 가 J- COD 가

[7]

### 2.2.2

GE/EPRI LBB COD [3]. , GE/EPRI  
 COD J- (global parameter) - 가  
 , COD (local parameter)  
 가 COD 가 , LBB COD  
 COD 가

$$\frac{e}{e_{p0.2}} = \left( \frac{s}{s_y} \right)^n \quad \text{for } s \geq s_y \quad (13)$$

,  $e_{p0.2}$   $s_y$  0.2% (8) 0.2%

$n$   $s_y/s_u$  (13) 가

### 2.2.3

GE/EPRI COD  $(a_e)$   
 COD 가 R6 가 2 [4]

$$W = \frac{1}{2} \frac{L_r^2 s_{ref}}{E e_{ref}} \quad (14)$$

(14) (7)  
 Kastner [8] Irwin , Wüthrich  
 [9] Dugdale 가 가 (14)

## 3. GE/EPRI J- COD

### 3.1

#### 3.1.1

TP304 SA312 TP316 . SA312 TP304 SA312  
 (quasi-static) , SA312 TP316 20 288 50

. Fig. 2~Fig. 4

Table 1

3.1.2

Fig. 1  
 355.6mm, 35.7mm,  $R_m/t$  4.48, 12.5%( $q$ )  
 / $p=0.125$ ) 40%( $q$  / $p=0.4$ ) 가 가

3.1.3

Fig. 5  
 1/4, 20, ABAQUS  
 [10], (20-nodes isoparametric brick reduced  
 integration element) 936, (small strain analysis)  
 2가 Fig. 2~Fig. 4, 6가  
 J- COD

3.2 GE/EPRI

GE/EPRI J- COD  
 Ramberg-Osgood  $a$   $n$

$$\frac{\mathbf{e}}{\mathbf{e}_o} = \frac{\mathbf{s}}{\mathbf{s}_o} + a \left( \frac{\mathbf{s}}{\mathbf{s}_o} \right)^n \quad (15)$$

,  $\mathbf{s}_o$  (yield strength)  $\mathbf{e}_o$

Ramberg-Osgood 가 GE/EPRI  
 가 3가 (Fit A), 5%  
 (Fit B)[11]. 0.1%  
 0.8 $\mathbf{e}_u$  (Fit C)[12].  
 ROFIT [13]. Fig. 2~Fig. 4

Table 2

SA312 TP304 SA312 TP316, Ramberg-Osgood  
 “Fit A”가  
 3가 가  
 SA312 TP316 가  
 Ramberg-Osgood 가, GE/EPRI J- COD

Table 1 Material properties for the analyses

	TP304 (50 )	TP316 (288 )	TP316 (20 )
$E$ (GPa)	204	190	206
$s_y$ (MPa)	269	165	234
$s_u$ (MPa)	559	455	545
$n$	0.3	0.3	0.3

Table 2 Ramberg-Osgood curve-fitting results

	TP304 (50 )		TP316 (288 )		TP316 (20 )	
	$a$	$n$	$a$	$n$	$a$	$n$
Entire curve (Fit A)	7.33	3.52	8.42	2.92	10.23	2.96
Up to 5% (Fit B)	5.97	4.30	5.76	4.11	3.39	4.72
0.1%- 0.8 $e_u$ (Fit C)	4.22	4.72	6.26	3.46	4.77	3.82

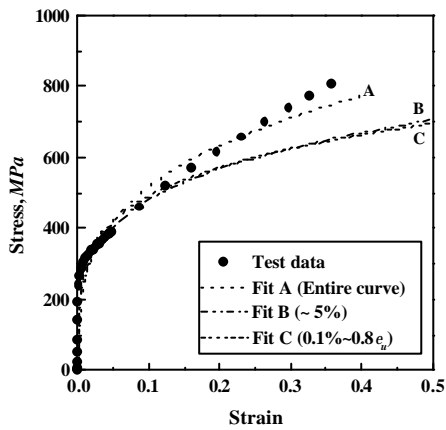


Fig. 2 Stress-strain curve and three different fitting results for SA312 TP304 (50 )

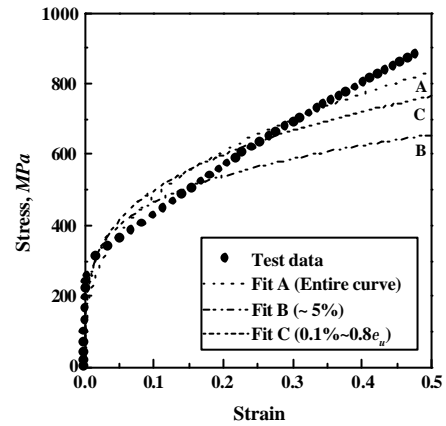


Fig. 4 Stress-strain curve and three different fitting results for SA312 TP316 (20 )

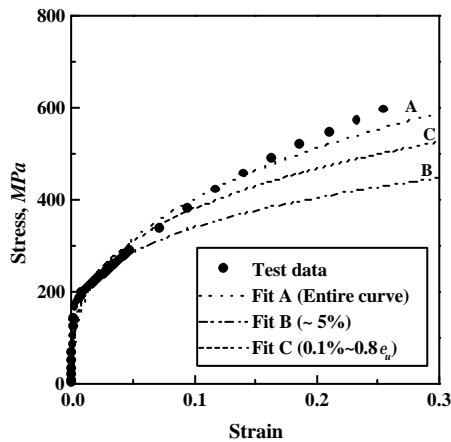


Fig. 3 Stress-strain curve and three different fitting results for SA312 TP316 (288 )

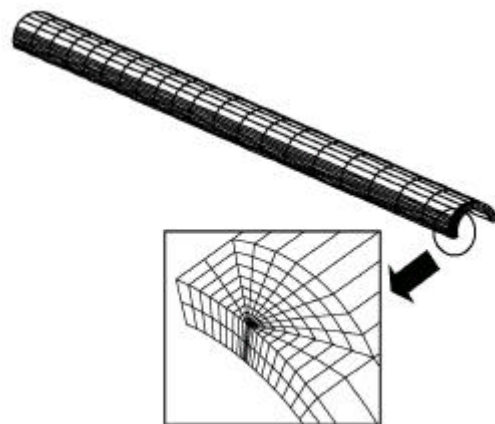


Fig. 5 A 3-D FE mesh for the circumferentially through-wall cracked pipe

Table 3 Summary of pipe test data

Loading	Test No.	Material	$D_o$ (mm)	$t$ (mm)	$R_m/t$	$q/p$	Temp. (°C)
Pure Bending	GE/1/B	304 SS	114.3	8.6	6.12	0.25	20
	GE/3/B	304 SS	114.3	8.6	6.12	0.5	20
	NRC/4111/1	A333 Gr. 6	114.3	8.9	5.93	0.37	288
	4.3-1*	STS-49	763.5	38.2	9.5	0.166	300
	3.3-1*	STS-410	166.0	14.5	5.22	0.166	300
Tension	GE/3/90/T	304 SS	114.3	8.6	6.12	0.25	20
Pressure	4121-1*	304 SS	168.1	12.9	6.02	0.386	288

\* These data are extracted from (ref. 14). All other data are from (ref. 3).

$$J = \frac{K^2(a_e)}{E'} + \alpha s_o e_o R_m (p - q) \frac{q}{p} \cdot h_1 \cdot \left[ \frac{M}{M_o} \right]^{n+1} \quad (16)$$

$$d = \frac{4M a_e}{p R_m^2 t E} \cdot V_1(a_e) + \alpha e_o a \cdot h_2 \cdot \left[ \frac{M}{M_o} \right]^n \quad (17)$$

(16) factor),  $M$  (17)  $K$ ,  $M_o$  (stress intensity factor)

$$M_o = 4s_o R_m^2 t \left[ \cos\left(\frac{q}{2}\right) - \frac{1}{2} \sin q \right] \quad (18)$$

(16) (17)  $V_1$   $h_1, h_2$  가  
[1,5].  $J$ - COD (effective crack length)

$$a_e = a + \frac{1}{bp} \left( \frac{n-1}{n+1} \right) \left[ \frac{K(a)}{s_o} \right]^2 \left[ 1 + \left( \frac{M}{M_o} \right)^2 \right]^{-1} \quad (19)$$

$b=2$ ,  $b=6$

$b=2$

[5].

#### 4.

##### 4.1

[3,14] COD 가 Table 3 Fig. 6~Fig. 12  
COD 가 COD (7) 2 가



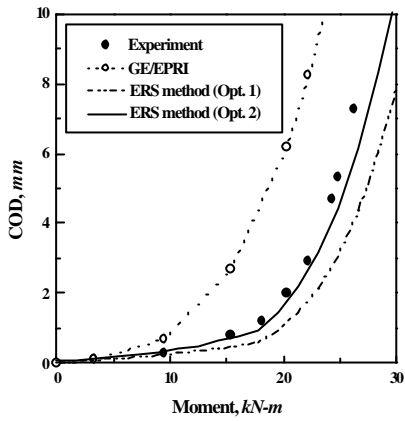


Fig. 6 Comparison of the COD predictions with pipe test data (GE/1/B, See Table 3)

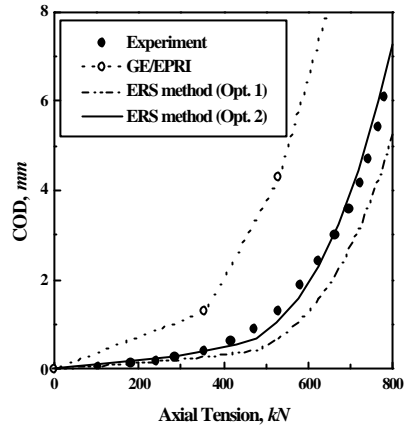


Fig. 9 Comparison of the COD predictions with pipe test data (GE/3/90/T, See Table 3)

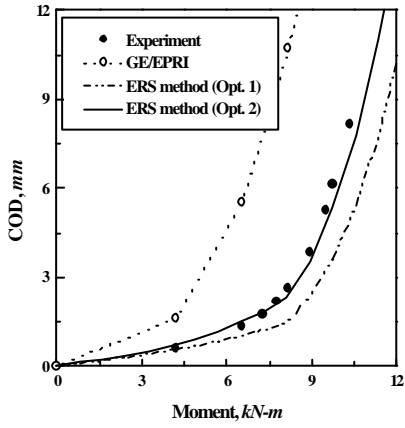


Fig. 7 Comparison of the COD predictions with pipe test data (GE3/B, See Table 3)

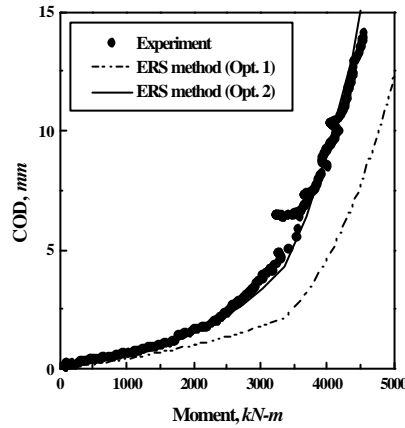


Fig. 10 Comparison of the COD predictions with pipe test data (4.3-1, See Table 3)

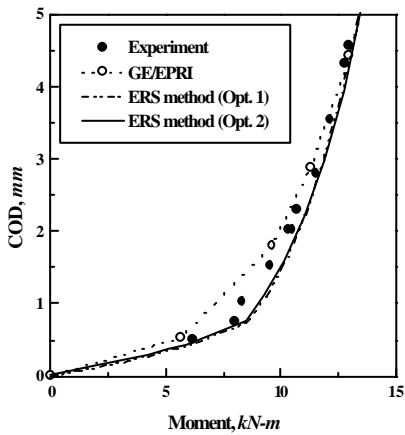


Fig. 8 Comparison of the COD predictions with pipe test data (NRC/4111/1, See Table 3)

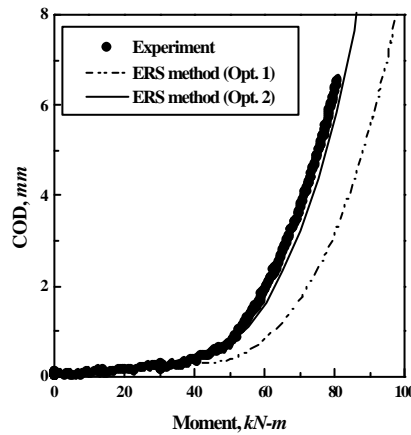


Fig. 11 Comparison of the COD predictions with pipe test data (3.3-1, See Table 3)

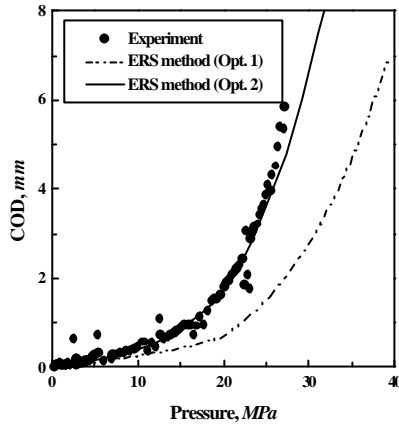


Fig. 12 Comparison of the COD predictions with pipe test data (4121-1, See Table 3)

(10) 1 가 GE/EPRI ERS COD 1  
 “O” 가 2 Fig. 6~Fig. 9 ERS  
 GE/EPRI  
 2 가

**4.2 GE/EPRI**

Fig. 13~Fig. 20 J- COD ERS GE/EPRI (2가 )  
 (3가 ) 6가 SA312 TP316 SA312  
 가 TP304(50 ) SA312 TP316(20 )  
 2 ERS Table 2  
 GE/EPRI Ramberg-Osgood  
 J- COD GE/EPRI  
 Ramberg-Osgood LBB GE/EPRI J- COD 가  
 3가 가 “Fit A” 가  
 , J- COD “Fit A” 가  
 가 SA312 TP304 “Fit C”  
 , SA312 TP316 “Fit B”  
 가 GE/EPRI J-  
 COD 가 Ramberg-Osgood  
 ERS J- COD GE/EPRI  
 COD GE/EPRI ERS

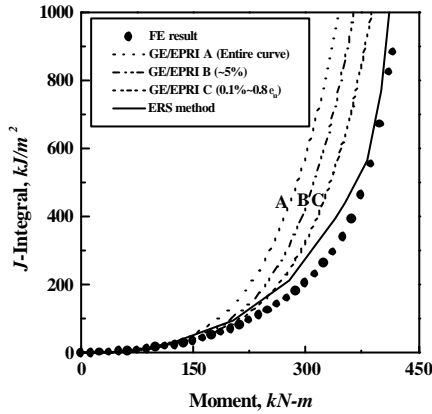


Fig. 13 Comparison of FE  $J$  values with those from engineering estimation scheme for SA312 TP304 (50 ,  $q/p = 0.4$ )

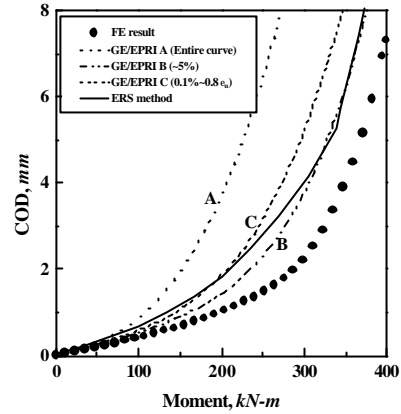


Fig. 16 Comparison of FE COD values with those from engineering estimation scheme for SA312 TP316 (20 ,  $q/p = 0.4$ )

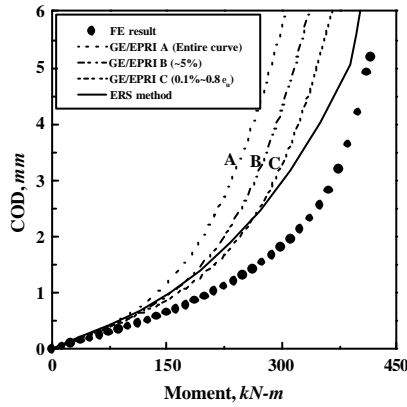


Fig. 14 Comparison of FE COD values with those from engineering estimation scheme for SA312 TP304 (50 ,  $q/p = 0.4$ )

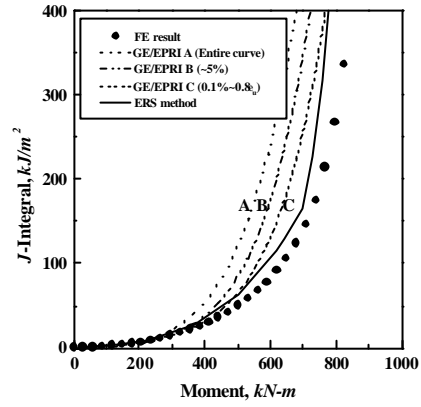


Fig. 17 Comparison of FE  $J$  values with those from engineering estimation scheme for SA312 TP304 (50 ,  $q/p = 0.125$ )

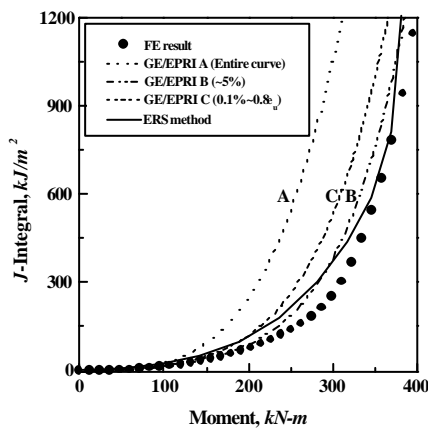


Fig. 15 Comparison of FE  $J$  values with those from engineering estimation scheme for SA312 TP316 (20 ,  $q/p = 0.4$ )

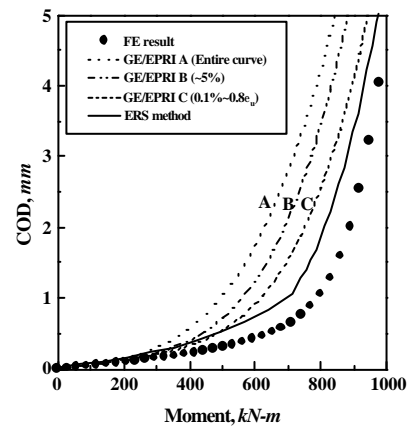


Fig. 18 Comparison of FE COD values with those from engineering estimation scheme for SA312 TP304 (50 ,  $q/p = 0.125$ )

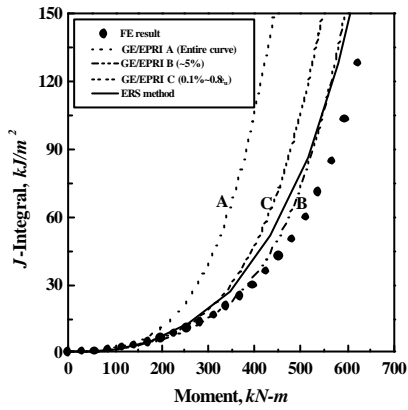


Fig. 19 Comparison of FE  $J$  values with those from engineering estimation scheme for SA312 TP316 (20,  $q/p = 0.125$ )

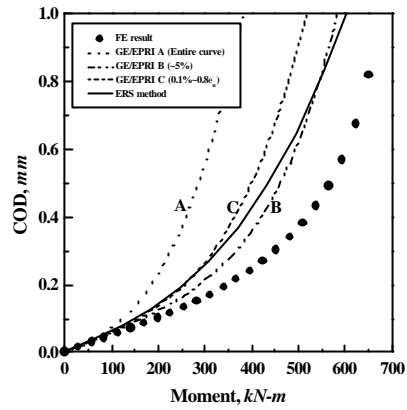


Fig. 20 Comparison of FE COD values with those from engineering estimation scheme for SA312 TP316 (20,  $q/p = 0.125$ )

5.

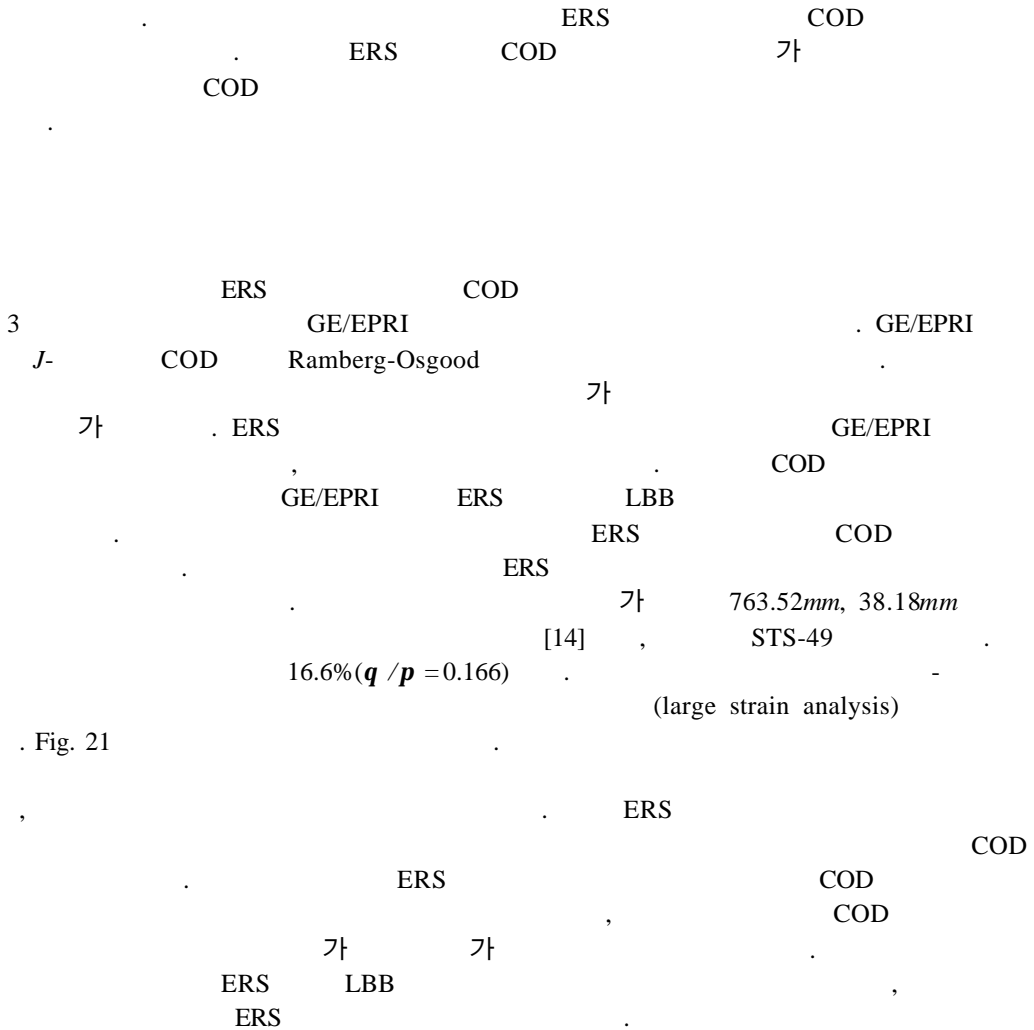


Fig. 21

[14], 763.52mm, 38.18mm  
STS-49  
(large strain analysis)



Wall Pipe Cracks," EPRI Special Report NP-5959-SR.

[4] 1999, "R6: Assessment of the Integrity of Structures Containing Defects," Revision 3, British Energy Generation Ltd.

[5] 1995, "Refinement and Evaluation of Crack-Opening-Area Analyses for Circumferential Through-Wall Cracks in Pipes," NUREG/CR-6300, USNRC.

[6] Miller, A.G. and Ainsworth, R.A., 1989, "Consistency of Numerical Results for Power-Law Hardening Materials and the Accuracy of the Reference Stress Approximation for J," Engineering Fracture Mechanics, Vol. 32, pp. 237-247.

[7] Kim, Y.J., 1999, "Reference Stress Approximations for J and COD of Circumferential Through-Wall Cracked Pipes," EPD/GEN/REP/0462/99, British Energy Generation Ltd.

[8] Kastner, W., Röhrich, E., Schmitt, W. and Steinbuch, R., 1981, International Journal of Pressure Vessels and Piping, pp. 197-219.

[9] Wüthrich, C., 1983, "Crack Opening Areas in Pressure Vessels and Pipes," Engineering Fracture Mechanics, Vol. 18, pp. 1049-1057.

[10] 1999, "ABAQUS User's manual," Hibbitt, Karlson & Sorensen, Inc.

[11] Norris, D.M. and Chexal, B., 1987, "PICEP : Pipe Crack Evaluation Program," EPRI NP 3596-SR.

[12] 1996, "Pipe System Experiments with Circumferential Cracks in Straight-Pipe Locations," NUREG/CR-6389, USNRC.

[13] 1997, "Computer Program to Calculate Ramberg-Osgood Parameters for a Stress-Strain Curve," Pipe Fracture Encyclopedia, Vol. 1, Battelle.

[14] 1997, "Pipe Fracture Test Data," Pipe Fracture Encyclopedia, Vol. 3, Battelle.